Ultrasound in Med. & Biol., Vol. 30, No. 10, pp. 1297-1306, 2004
Copyright © 2004 World Federation for Ultrasound in Medicine & Biology
Printed in the USA. All rights reserved
0301-5629/04/$–see front matter

ELSEVIER

doi:10.1016/j.ultrasmedbio.2004.07.012

● *Original Contribution*

SIMULATION STUDY OF EFFECTS OF SPEED OF SOUND AND ATTENUATION ON ULTRASOUND LATERAL RESOLUTION

QUAN CHEN and JAMES A. ZAGZEBSKI
Department of Medical Physics, University of Wisconsin-Madison, Madison, WI, USA

(*Received* 24 *March* 2003, *revised* 25 *June* 2004, *accepted* 22 *July* 2004)

Abstract—Experiments have shown that the lateral profile of a point target measured with a clinical ultrasound scanner is wider when the target is embedded in a urethane phantom than when it is in a traditional gel phantom. The behavior has been attributed to the low speed of sound in the urethane material, with the possibility that some of the broadening is caused by increased attenuation in this material. In this paper we apply a computer simulation model to study this behavior. Lateral beam profiles modeled for targets within a medium having a speed of sound and an attenuation matching that of urethane are compared with profiles for targets in a water-based gel. Simulations yield results that agree qualitatively with published experimental results. The lateral profile broadening in urethane is caused by the 6 % mismatch between speed of sound in this material and the speed of sound assumed in the receive focusing and beam forming. Attenuation plays a lesser role than the mismatch of the speed of sound. (E-mail: jazagzeb@facstaff.wisc.edu) © 2004 World Federation for Ultrasound in Medicine & Biology.

Key Words: **Speed of sound, Attenuation, Resolution, Simulation, Ultrasound quality control, Urethane phantom.**

INTRODUCTION

Ultrasound (US) phantoms are commonly used for equipment acceptance tests and routine quality assurance (QA) measurements. The phantoms are meant to be "tissue-mimicking" so that their measurement results are consistent with clinical performance. Generally, this means that their contents should have a speed of sound of approximately 1540 m/s and an attenuation of approximately 0.5-0.7 dB/cm/MHz.

Recently, urethane rubber phantoms have appeared in the market place. Compared to most commonly used water based gel phantoms, urethane phantoms do not dry out and have a longer life. However, the sound speed in urethane phantoms is generally between 1430 m/s and 1480 m/s, which is approximately 6% lower than the propagation speed assumed in the calibration of ultrasound scanners. Moreover, the frequency-dependence of attenuation is high ($f^{1.6}$ compared to $f^{1.1}$) (Zagzebski and Madsen 1995) compared to that in water based gel phantoms.

Address correspondence to: James Zagzebski, Department of Medical Physics, University of Wisconsin-Madison, 1530 MSC, 1300 University Ave., Madison, WI 53706, USA. E-mail: jazagzeb@facstaff.wisc.edu

Goldstein (2000) examined the effect of acoustic velocity errors on distance measurement and resolution assessments done with phantoms. The difference in speed of sound causes small mis-registrations of image location. Goldstein also noticed that ultrasound beam widths in urethane rubber phantoms were almost double those measured using water-based gel phantoms. This beam widening is suggested to come potentially from two sources. One is the difference in attenuation between the two media. Since the attenuation of urethane rubber phantoms has a stronger frequency dependence than attenuation in most water-based gel phantoms, the pulse average frequency would be lower due to the increased attenuation of higher frequencies. Lower frequencies, in turn, lead to wider beam widths. Another source of increased beam widths is the lower speed of sound in the urethane material. The difference between the actual speed of sound in the medium and the assumed one in setting up the beam former in the scanner will cause beam defocusing, making the beam wider than when the sound speed in the medium and that assumed in the beam former are matched. The mechanism is discussed in more detail later in this paper.

At this point, it is not clear what the relative contribution of these two effects is. Dudley et al. (2002) studied the effect of speed of sound on resolution by

imaging point-like targets in water at different temperatures. They showed a broader beam profile in media with lower propagation speeds, both in the presence and absence of significant attenuation. However, because they did not have total control over all factors governing acoustic properties of the media, Dudley et al. (2002) could not provide conclusive evidence that the difference in beam profiles observed was due only to the speed of sound difference.

This paper applies computer simulations to study the effects of speed of sound and attenuation in the medium on lateral resolution estimates of ultrasound scanners. We have developed a computer model (Li and Zagzebski 1999) to simulate imaging for ultrasound array transducers. This model calculates ultrasound fields in the frequency domain. It takes into account the effects of frequency-dependent attenuation, backscattering, and dispersion, and it includes beam-forming techniques such as apodization, dynamic aperture, elevational focusing, multiple transmit focusing, and dynamic receive focusing. The advantage of computer simulations is that we have total control over the simulated phantom properties and imaging conditions. This will help identify the contributions of each factor.

THEORY

Transmit focusing

Most ultrasound scanners use electronic focusing techniques applied to array transducers when generating the ultrasound field. Time delays are applied to pulses sent to transducer elements so that the signals transmitted from individual elements will arrive at a designated position in phase. For a linear or phased array, the time delay needed for the nth element to focus the beam at F_z can be represented as (Li and Zagzebski 1999):

$$t(n, F_z) = \frac{1}{c}\left(\sqrt{\left[(n - (N+1)/2)d\right]^2 + F_z^2} - F_z\right), \qquad (1)$$

where c is the speed of sound, N is the number of array elements in the active aperture, d is the center-to-center distance between elements, and the value of n ranges from 1 to N. For most clinical scanners, the speed of sound c is assumed to be 1540 m/s when calculating the required time delays for a certain focal distance. In actual cases where the speed of sound of the medium is different, the focus will be shifted. Figure 1 illustrates this behavior where it is assumed that the focus is set at F. The required time delay is calculated from the assumed sound speed, 1540 m/s. w illustrates the wave front of the sound beam under this assumed speed of sound. However, when the speed of sound of the medium is less than the assumed speed of sound, the actual wave front is illustrated by w', and the actual focus is located at F', farther than the designated position.

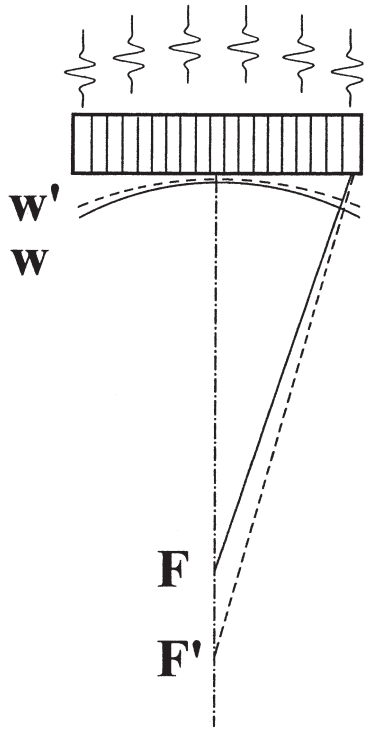

Fig. 1. Effect of speed of sound on transmit focus. The time delay of each transducer element is set such that the wavefront would follow W and the sound beam would focus at F under a 1540 m/s medium sound speed. With a decreased medium sound speed, the same time delay would produce a wavefront of W' and focus at F'.

The amount of shift can be estimated as follows. The assumed time delay will be the same both for the assumed speed of sound $c_0 = 1540$ m/s and for the actual speed of sound c'. The assumed focus is F_0, but the actual focus is F'. We have: for $n = 1 \cdots N$,

$$\frac{1}{c_0}\left(\sqrt{\left[(n - (N+1)/2)d\right]^2 + F_0^2} - F_0\right) = \frac{1}{c'}\left(\sqrt{\left[(n - (N+1)/2)d\right]^2 + F'^2} - F'\right). \qquad (2)$$

When $F_0 > [(n - (N + 1)/2)d]$, eqn (2) reduces to

$$F' = \frac{c_0}{c'}F_0. \qquad (3)$$

Note this is the same expression as the mis-registration of a point target. This new focus F' is an imperfect focus since the assumption can not be met for all elements, and eqn (2) can not be satisfied exactly.

Dynamic receive focusing

Virtually all ultrasound scanners use dynamic receive focusing during the echo reception process. Immediately after the transmit pulse, receive-focus time delays for each array element are set for focusing at a shallow depth. Then, in real time, as echoes arrive from deeper and deeper structures, the receive focal length is increased automatically by adjusting the time delays for each array element. The value of the receive focal length F is determined from the echo time of flight t_{tof} as:

$$F = c_0 t_{tof} / 2. \tag{4}$$

Consider a point target located at depth d inside a medium with a speed of sound c_0. The echo time of flight, t_{tof} from this point target is $2d/c_0$. Therefore, when the echo is received, the receive focal length is set at $F = c_0 t_{tof}/2 = d$, exactly the same location as the point target. This results in the sharpest possible image of the target.

Now, consider the same point target in a medium with a speed of sound c'. The echo time of flight t_{tof} is $2d/c'$. When the echo is received, the time delay of each element is set automatically by the beam-former such that it will produce a focal length of $F = c_0 t_{tof}/2 = d \cdot c_0/c'$. The beam-former calculates the time delay necessary using eqn (1). However, since the beam-former always assumes the medium has a sound speed of $c_0 = 1540$ m/s, and the actual medium that the sound propagates in has a speed of sound of c', using eqn (3), we have the actual focus located at

$$F' = \left(\frac{c_0}{c'}\right)^2 d. \tag{5}$$

This location is different from the actual position of the point target. This process is illustrated in Fig. 2. For a 6% difference in speed of sound, the receive focus will miss the target by approximately 12% of its depth. The result will be an increase in the received beam width at the target.

Pulse-echo beam width

For pulse-echo imaging, the combined effect of the transmit and receive fields can be modeled as (Li and Zagzebski 1999):

$$A^{TR}(\boldsymbol{r}, \omega) = A^{T}(\boldsymbol{r}, \omega) A^{R}(\boldsymbol{r}, \omega) \tag{6}$$

where $A^{T}(\boldsymbol{r},\omega)$ models the transmit profile, and $A^{R}(\boldsymbol{r},\omega)$ models the receiving profile. For illustration, let us approximate the beam's lateral profile with a Gaussian function. Therefore, we have:

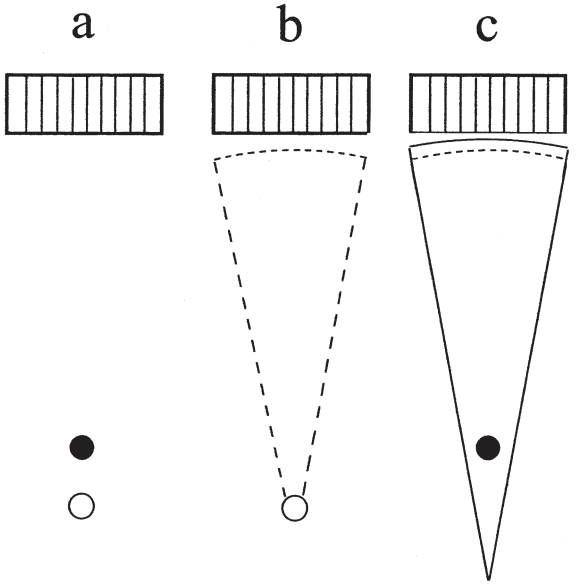

Fig. 2. Illustration of the mis-focus during dynamic receive focusing assuming the medium speed of sound is lower than the assumed 1540 m/s. The solid circle represents the real-space location of the target, and the open circle represents the image location of the target. (a) The pulse-echo time is longer under a lower medium sound speed, making the target appear to be in a deeper position. (b) The dynamic focusing circuit adjusts the time delay of each element so that the transducer would focus at that deeper position, if the medium sound speed is assumed 1540 m/s. (c) In reality, the medium sound speed is lower, so the real focus is at a deeper position.

$$\exp\left(-\frac{\rho^2}{\sigma_T^2}\right) = \exp\left(-\frac{\rho^2}{\sigma_T^2}\right)\exp\left(-\frac{\rho^2}{\sigma_R^2}\right). \tag{7}$$

where ρ is the lateral position, σ_{TR}, σ_T, and σ_R are measures of beam width for the pulse-echo field, the transmit field, and the receive field respectively. From eqn (7), we get a relationship to convert the transmit beam width and the receive beam width to pulse-echo beam width as:

$$\frac{1}{\text{width}_{TR}^2} = \frac{1}{\text{width}_{T}^2} + \frac{1}{\text{width}_{R}^2}. \tag{8}$$

Eqn (8) means the pulse-echo beam width will be decided primarily by the narrower beam if the transmit and receive beam widths are significantly different.

Frequency dependent attenuation

For most biological tissues the ultrasound attenuation is nearly proportional to frequency (Bamber 1986). As a result of this property, when an ultrasound pulse propagates through tissue, higher frequency components of the pulse are preferentially attenuated, reducing the effective frequency with increasing depth.

The amount of frequency shift can be easily predicted if we consider the frequency spectrum of the ultrasound pulse as a Gaussian, a common approach followed by many investigators. If the attenuation of the tissue is proportional to frequency, f, the echo spectrum after traveling a total distance z is:

$$S_r(f) = S_0 e^{-\frac{(f-f_0)^2}{\sigma^2}} e^{-\alpha_0 f z}, \quad (9)$$

where S_0 is the unattenuated spectrum, f_0 is the original center frequency, and α_0 is the attenuation coefficient in units of 1/cm/MHz. Further derivation shows the attenuated spectrum is still Gaussian shaped. The center frequency of this new spectrum is calculated as:

$$f_c' = f_0 - \frac{\alpha_0 z \sigma^2}{2} = f_0\left(1 - \frac{\alpha_0 z f_0}{8 \ln 2} BW^2\right), \quad (10)$$

where BW stands for fractional bandwidth. Now, if the attenuation of the medium exhibits a f^2-dependence, with attenuation coefficient α_1 having the units of 1/cm/MHz^2, the echo spectrum after propagating a total distance z is:

$$S_r(f) = S_0 e^{-\frac{(f-f_0)^2}{\sigma^2}} e^{-\alpha_1 f^2 z}. \quad (11)$$

Further derivation shows that it is also Gaussian shaped. The center frequency of this new spectrum is:

$$f_c'' = \frac{1}{1 + \alpha_1 z \sigma^2} f_0. \quad (12)$$

When $\alpha_1 z \sigma^2 < 1$, eqn (12) will reduce to

$$f_c'' = f_0(1 - \alpha_1 z \sigma^2) = f_0\left(1 - \frac{\alpha_1 z f_0^2 BW^2}{4 \ln 2}\right). \quad (13)$$

Eqns. (10) and (13) tell us that the attenuation will cause the center frequency to shift to a lower frequency. The amount that it shifts will be proportional to the actual attenuation value at the center frequency and the square of the pulse bandwidth. For a f^2-dependence of attenuation, the shift will be twice that of the linear dependence of attenuation on frequency.

With the relation between the beam width at the focal distance and wavelength, (Zagzebski 1996) we have:

$$\frac{\text{width}_{\text{new}}}{\text{width}_{\text{old}}} = \frac{f_{\text{old}}}{f_{\text{new}}}, \quad (14)$$

which means a decrease in center frequency will cause a proportional increase in beam width.

SIMULATION METHODS

The computer simulation program developed by our group has been described in detail (Li and Zagzebski 1999). For the present study, we modeled a linear array consisting of elements of size 0.15 mm by 10 mm, with a center-to-center distance of 0.2 mm. Each beam line is formed using 128 consecutive elements. In most array transducers, a fixed elevational focus is applied using a mechanical lens in contact with each array element. The transmit focus may be at a different location from the elevational focus, but for this simulation, we set the elevational focus to be the same as the lateral transmit focus. This elevational focus does not change by dynamic receive focus. During the dynamic receiving process, the aperture was simulated as changing dynamically with depth so that a constant F-number of 2 was maintained until it reached a limit of 128 elements. A Gaussian-shaped input pulse with a center frequency of 5 MHz and a bandwidth of 50% was used in the simulation.

In addition to the array focusing parameters, the model requires input of the speed of sound and the attenuation properties of the medium, as well as positions of simulated scatterers. In this study, we represented the phantom as having a column of discrete point targets at 5 mm intervals over an 80 mm depth range. We modeled a second phantom by shifting the point targets in the first phantom by 2.5 mm for finer sampling. The resultant simulated RF signal was then envelope-detected and log-compressed to form a B-mode image. Time gain compensation (TGC) was applied to the simulated echo data to achieve an equal mean echo signal brightness at each depth. TGC was implemented in the following way. For each dB-scaled point target image, we first determined the peak echo amplitude; then we calculated its difference from a preset value that did not vary with depth. Then we subtracted this difference value for the entire region surrounding the point target so that the peak brightness equaled our preset value. Since this process was applied to a log-compressed image, the subtraction and addition is equivalent to minify and magnify the envelope signal. The process was repeated for every point target, yielding an equal peak brightness for each point target image.

A typical point target simulated image (not at the transmit focus) is displayed over a 30 dB dynamic range in Fig. 3. The image of the point target spreads in both directions due to the lateral profile of the beam. Because of the different locations of the transmit and receive foci, the image consists of two spreading lines, forming an "X" pattern. Our analysis consisted of computing pulse-echo response widths for each target, consistent with experimental approaches (Goldstein 2000; Dudley et al. 2002). To make the pulse-echo width measurement, we first calculated the maximum intensity value along each vertical line. Then we constructed a lateral profile with these maxima, and finally measured its width. Using this

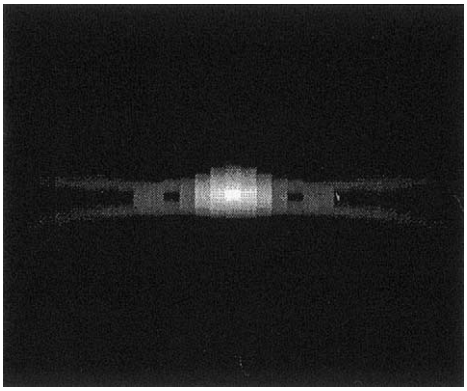

Fig. 3. A typical point target image. Note the spreading on both sides.

method, we took into account beam spreading as an interpreter's eyes would normally do. The width measurement is normally taken at the –15dB level. Note that Dunley et al. measured FWHM (full-width-half-maximum) value of the pulse-echo response. However, they made measurements on frame-grabbed B-mode images, which are generated after echo signals are log-compressed. Therefore, our –15 dB width is similar to their FWHM if the B-mode image is displayed with a 30 dB dynamic range.

RESULTS

Figure 4 shows examples of simulated images of point targets used to measure beam widths. The images are displayed over a 30 dB dynamic range. A 5.0 MHz, 50% bandwidth pulse was used in the simulation. The different panels show the effects of using a single fixed transmit and receive focus at 4 cm [Fig. 4a]; single fixed transmit focus at 4 cm, and a continuous receive focus, with a fixed receive F number of 2 in the near field in a medium with no attenuation, and a speed of sound of 1540 m/s [Fig. 4b], 1450 m/s [Fig. 4c], and 1630 m/s [Fig. 4d], both with continuous receive focus. Figure 4a shows that a tightly focused ultrasound beam will converge towards and diverge beyond the focus. However, as Figure 4b demonstrates, when dynamic receive focusing is used, the image widths of point targets are dramatically reduced at all depths. This is consistent with images of point targets generated experimentally using clinical scanners and array transducers. Figure 4c and d demonstrate that either a decrease or an increase in the speed of sound from the value for which the machine is calibrated would both result in an increase in the image width at most depths.

To study the effect of the speed of sound of the medium on focusing, we ran our simulation to assume a single transmit and receive focus, both located at a depth

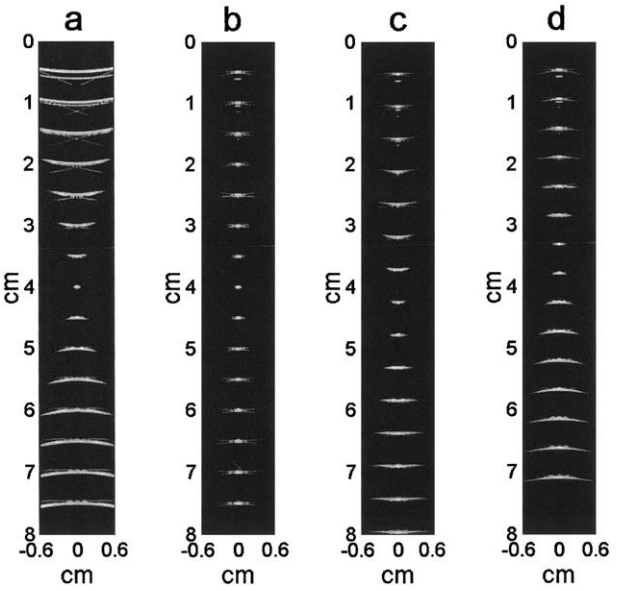

Fig. 4. Simulated B-mode images. (a) single fixed transmit and fixed receive focal depth at 4 cm in a medium sound speed of 1540 m/s; and single fixed transmit focus at 4-cm and dynamic receive focus in a medium sound speed of (b) 1540 m/s; (c) 1450 m/s; and (d) 1630 m/s. It is assumed that there is no attenuation in the medium.

of 4 cm. Figure 5 shows the –15 dB pulse-echo response width of a point target, plotted as a function of the actual target depth for this fixed focus. For simplicity, we only plotted the result for a 1540 m/s and a 1450 m/s medium speed of sound. The image width was cut off at 1.2 cm due to the dimension we specified in the simulation.

The only difference we observe between the point target image widths for a 1450 m/s and a 1540 m/s sound speed when a fixed transmit-receive focus is used is that

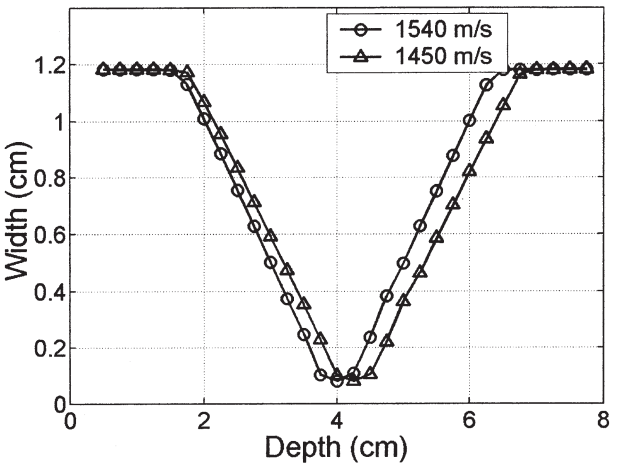

Fig. 5. Point target –15 dB image widths vs. depth under a fixed transmit and receive focal depth of 4 cm.

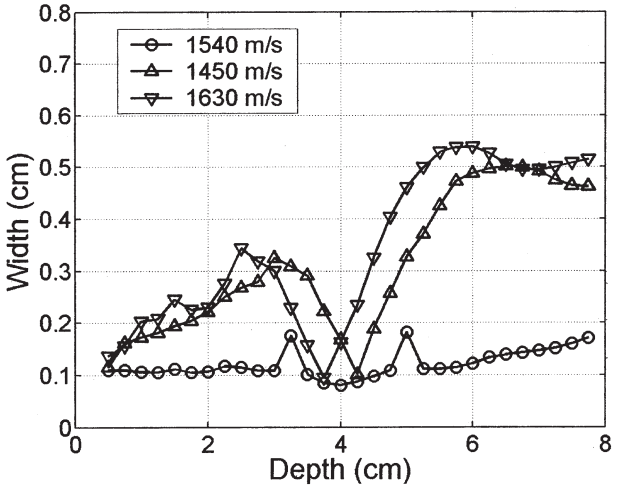

Fig. 6. Point target –15 dB image widths vs. depth under a fixed transmit focal depth of 4 cm and dynamic receive focus.

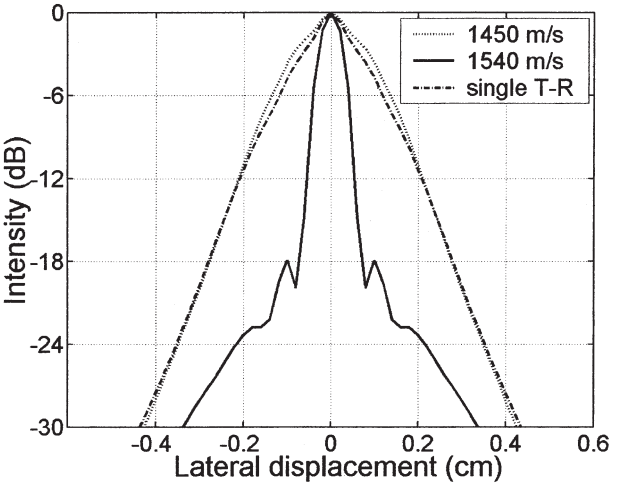

Fig. 7. Lateral profile of a point target image. The solid curve is the profile obtained for a medium sound speed the same as the assumed 1540 m/s. The dotted curve is the profile obtained for a medium sound speed of 1450 m/s. The dash-dot curve is the profile obtained at a medium sound speed of 1540 m/s but with single fixed receive focus rather than dynamic receive focus as used in the previous two curves. The single fixed receive focus is selected to correspond to the mis-focus in a medium sound speed of 1450 m/s.

the 1450 m/s curve is a stretched version of the 1540 m/s curve. The beam's actual focal depth is moved from 4.0 cm to around 4.25 cm when the speed of sound changes from 1540 m/s to 1450 m/s. This agrees with the prediction from eqn (3). Also, from the fact that the beam width at the focus stays approximately the same, we can conclude that the "imperfection" of the focus is not significant for these conditions. Under our simulation condition, the F number would remain at 2 for a focal depth less than 5 cm and decrease below 2 for a deeper focal depth. As a result, the approximation we made during the derivation of eqn (3) has the same error for a focal depth less than 5 cm, but a lower error for a focal depth deeper than 5 cm. Therefore, we can rule out an "imperfect focus condition" as the cause of beam width increases for all depths in our simulation.

Figure 6 shows the point target image width plotted as a function of the actual depth in a medium with negligible attenuation and a speed of sound of 1540 m/s. Also shown are widths when the speed of sound is 1450 m/s, and 1630 m/s. A single transmit focus at 4 cm and dynamic receive focus was assumed in the simulation. The width is measured at 15 dB below the peak brightness at each depth. In contrast to results in Figure 5, for most depths, the target image width is significantly greater for sound speeds of 1450 m/s and 1630 m/s than it is for 1540 m/s. The 1540 m/s curve stays nearly constant for all depths, exhibiting ideal behavior for the constant F number. The response width gets slightly smaller at the transmit focus and rises a little at the end of the range considered. The two "spikes" around the focus are caused by interference of the side lobe at these two depths. In contrast, the 1450 m/s curve and 1630 m/s curves both rise fairly quickly as depth increases. The differences seem smaller around the transmit focus. This is similar to behavior reported by previous investigators (Goldstein 2000; Dudley et al. 2002).

To verify that the increase in pulse-echo response width in Fig. 6 is due to the mis-focus during receiving as described by Fig. 5, we simulated an image of a point target at a depth of 6 cm in a medium whose sound speed is 1450 m/s. Initially, the image was obtained with a machine that used 1540 m/s as the speed, a transmit focal distance of 4 cm, and dynamic receive focus. According to our analysis (Eqn 5), echoes received from a reflector at this depth in a 1450 speed of sound medium would be beam formed with time delays that apply to reflectors at a depth of 6.77 cm, resulting in a broader pulse-echo response width than if the medium had a sound speed of 1540 m/s. Figure 7 plots the lateral pulse echo response profile of the image of this target. In addition, the significantly narrower profile obtained if the target were in a medium having the "correct" speed of sound, 1540 m/s, also is shown. Finally the dashed line in Fig. 7 is the response profile for a target at a 6 cm depth in a medium with sound speed 1540 m/s but with a fixed transmit focus at 4.25 cm (the resultant transmit focal depth in the 1450 m/s medium, according to Eq. 3) and a fixed receive focal depth at 6.77 cm (the actual receive focal depth according to Eqn 5). The profile obtained with these adjusted focal depths in the 1540 m/s medium is in nearly perfect agreement with the original profile computed with dynamic receive focus when the target is in a medium having a 1450 m/s sound speed. The small

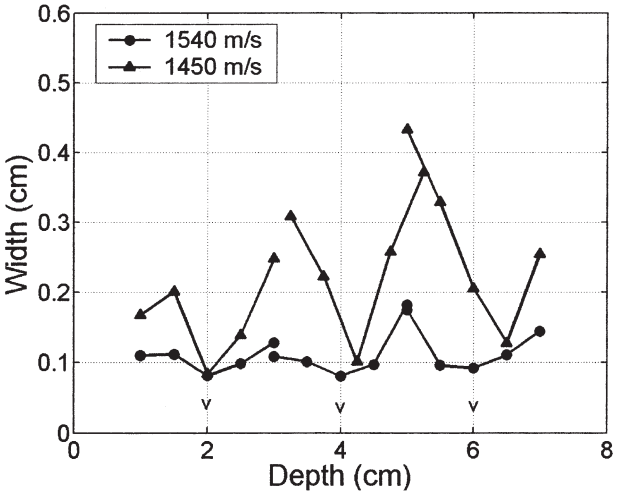

Fig. 8. Target image width vs. depth under multiple transmit focal zone conditions, both when the speed of sound in the medium matches that assumed in the beam former (1540 m/s) and when the medium speed of sound is 1450 m/s.

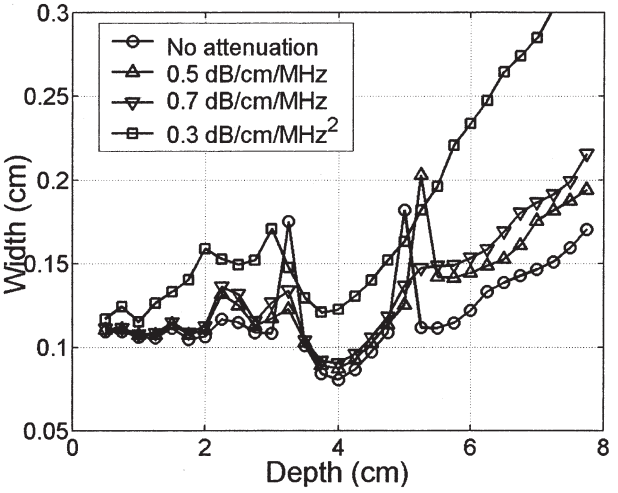

Fig. 9. Effect of attenuation on the target image width.

differences between the two curves are likely caused by differences in focus conditions. The focus is "imperfect" in the 1450 m/s dynamic receive focus case, but is perfect for the 4.25 cm transmit, 6.77 cm receive case in the 1540 m/s medium.

Figure 8 shows the effect of multiple transmit focal depths. The transmit focal depths were set at 2, 4, and 6 cm, with dynamic receive focus still applied for each of these zones. Note, the target image width around each focal zone is plotted separately. Comparing results with Fig. 6, the 1540 m/s curves have only a slight improvement under the multiple transmit focus condition. In contrast, for a speed of sound of 1450 m/s, the width is sharply reduced near the transmit focus. The behavior can be explained with the help of eqn (8). The correct receive focus for each point target in a 1540 m/s medium means that the receive beam width is the narrowest. Thus there will not be much room for improvement. However, for a medium having a sound speed of 1450 m/s, the mis-focus makes the receive beam width wider. At the position of the transmit focuses, the point target image width is reduced greatly due to the narrow transmit beam width. Note that this sharp narrowing happens only at the point of actual focus. Due to the speed of sound difference, the actual focus is different from the preset focus, as the graph shows. The graph also indicates that using multiple transmit focal zones helps to reduce the effect of speed of sound on the target image width. To get a smoother curve, more transmit focal depths are needed.

Effects of different amounts of attenuation in the simulations are shown in Fig. 9. The point target image width is plotted as a function of depth with no attenuation, 0.5 dB/cm/MHz, 0.7 dB/cm/MHz, and 0.3 dB/cm/MHz^2. The speed of sound assumed is 1540 m/s. A single transmit focal depth of 4.0 cm, and dynamic receive focus is simulated along with a 5 MHz, 50% bandwidth pulse. These plots show that the effect of attenuation alone on beam width is much smaller than the mis-focus effect caused by the difference in speed of sound.

Figure 10 shows the lateral profile of a point target at 6 cm imaged with different bandwidth pulses (10%, 50%, 100%, and 150%) and different attenuation coefficients (no attenuation, 0.5 dB/cm/MHz, and 0.3 dB/cm/MHz^2). When there is no attenuation present, as shown in Fig. 10a, there is no broadening of the beam profile as the bandwidth is increased. When there is attenuation, as shown in Fig. 10b and Fig. 10c, the beam is wider for broader bandwidths. This trend can be predicted by eqn (10), eqn (13), and eqn (14). However, the actual increase in width is not proportional to the square of the bandwidth like the approximations represented in these equations.

DISCUSSION

With computer simulations, we successfully reproduced the dependencies of displayed beam widths on speed of sound in the media that others have observed experimentally. The simulated B-mode image shown in Fig. 4b-d and the pulse-echo beam width vs. depth curve shown in Fig. 5 resemble the results obtained by Dudley et al. (2002).

The theory behind this phenomenon was presented in detail. Various simulations were run to check the validity of the theory. Using a transmit focus and a receive focus at the same depth, we are able to verify the shift of the focus and the focus condition when the speed of sound in the medium is different from that assumed during beam forming. In order to verify that

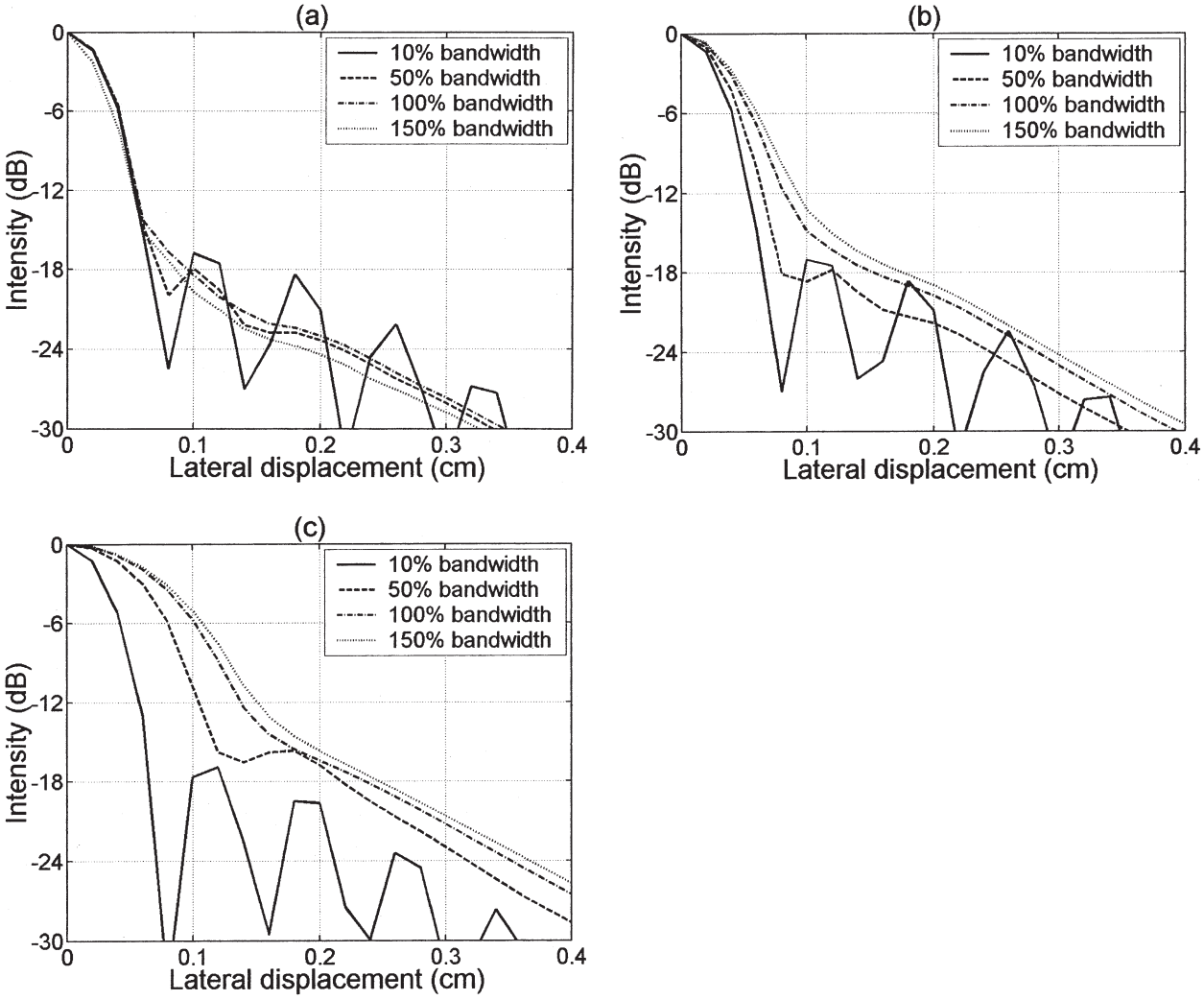

Fig. 10. Effect of bandwidth of the incident pulse on the lateral profile of a point target image in a medium with (a) no attenuation; (b) 0.5 dB/cm/MHz; (c) 0.3 dB/cm/MHz^2.

the increase in pulse-echo response width is due to the misplacement of the focus during the dynamic receiving process, we ran a simulation applying a single transmit focus and a single receive focus, both at the same depth. The lateral pulse-echo profile obtained from that simulation is virtually the same as obtained with dynamic receive focus. Therefore, this indicates that the increase in pulse-echo response width during normal imaging conditions (dynamic receive focusing) with an incorrect speed of sound is caused by the misplacement of the focus.

From the simple pulse-echo beam width profile shown in Fig. 5, we can predict the width of a single transmit – dynamic receive focus beam illustrated in Fig. 6. The width as a function of depth in Fig. 5 can be represented as a linear function with respect to the distance from the focus:

$$\text{width}(d) = \text{width}(F) + A \cdot |d - F|, \qquad (15)$$

where F is the focus, d is the depth, A is a constant factor, and width(F) is the width at the focus. From values in Fig. 5, we can estimate that $A = 0.4$ and width(F) $= 0.08cm$. Since the transmitting and receiving condition are the same in Fig. 5, with eqn (8), we have:

$$\text{width}_T(d) = \text{width}_R(d) = \sqrt{2}\text{width}(d) \qquad (16)$$

where the subscript T and R refer to transmit and receive. For the 1540 m/s curve in Fig. 6:

$$\text{width}_T(d) = \sqrt{2} \cdot (0.08 \text{ cm} + 0.4 \cdot |d - 4 \text{ cm}|), \qquad (17a)$$

and for the correct dynamic receive focus, $d = F$,

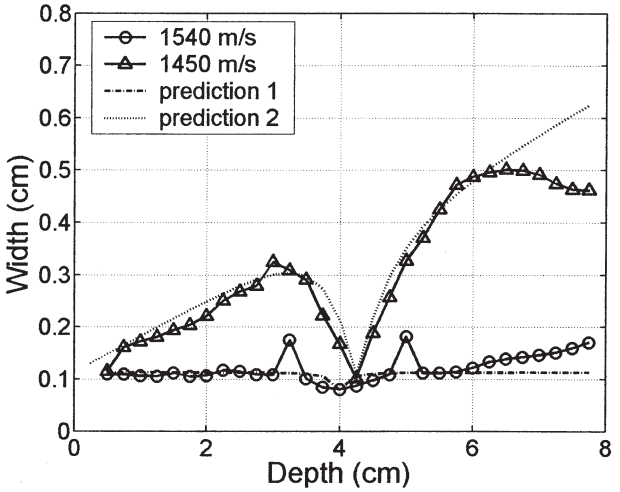

Fig. 11. Comparison between the simulated target image width for different medium sound speeds and predictions based on the result obtained with a fixed transmit and receive focus as shown in Fig. 5.

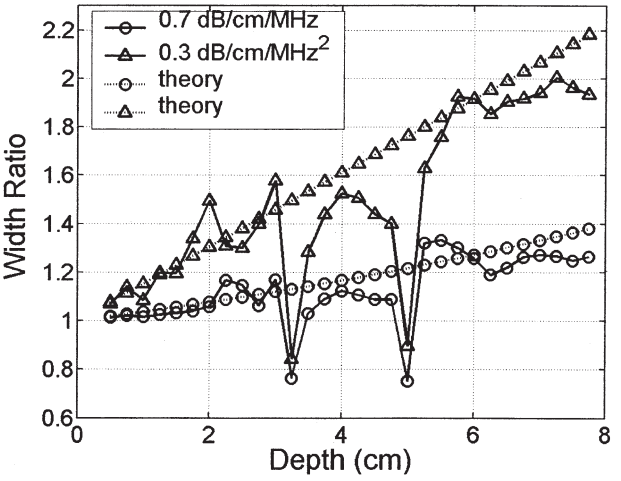

Fig. 12. Point target image width increase due to attenuation, obtained with simulations (solid curve) and with theoretical predictions (dotted curve). The change in point target image width is expressed in width ratios. The width ratio is defined as the ratio of the beam width obtained with medium attenuation to the width obtained without medium attenuation.

$$\text{width}_R(d) = \sqrt{2} \cdot 0.08 \ \text{ cm}, \tag{17b}$$

we can calculate the pulse-echo beam width from eqn (8). Similarly, for a medium with a speed of sound of 1450 m/s, 6% less than assumed value, the transmit focal depth is 4.25 cm and the receive focal depth can be calculated from eqn (5). We have:

$$\text{width}_T(d) = \sqrt{2} \cdot \left(0.08 \ \text{ cm} + 0.4 \cdot \left| d - 4.25 \ \text{ cm} \right|\right), \tag{18a}$$

and

$$\text{width}_R(d) = \sqrt{2} \cdot \left(0.08 \text{ cm} + 0.4 \cdot \left| d - d \cdot 1.06^2 \right|\right). \tag{18b}$$

From these two equations, we can calculate the pulse-echo beam width from eqn (8). We plotted the predictions calculated from eqn (17a, b) and eqn (18a, b), and display these with the actual simulation result in Fig. 11. As can be seen, the prediction fits the actual simulation well. It only deviates at deep depths where the aperture of the transducer is not enough to maintain an F-number of 2.

The simulation of beam width changes with attenuation also agrees with theory. From eqn (10), eqn (13), and eqn (14), we can calculate the ratio of the width as a function of depth. Figure 9 shows the beam width as a function of depth for different attenuation conditions. We chose two curves with different frequency dependencies, 0.7 dB/cm/MHz and 0.3 dB/cm/MHz^2. We calculated their ratio to the curve with no attenuation. The width ratio as a function of depth obtained from simulation data, as well as the theoretical prediction from eqn (10), eqn (13) and eqn (14) are plotted in Fig. 12. The prediction agrees with simulation very well in both cases. The interference from side lobes at 3 cm and 5 cm was magnified through this process.

On the other hand, the change in beam width with respect to changes in incident pulse bandwidth only agrees with theory qualitatively. As shown in Fig. 10a-c, the width will not change with bandwidth when there is negligible attenuation. When there is attenuation present, the increase in width is greater as bandwidth increases. These are all predicted by eqn (10), eqn (13), and eqn (14). However, the increase doesn't correspond well numerically with the square of the bandwidth. One plausible explanation is that the frequency shift is a continuous process, but eqn (10) and eqn (13) are valid only for small changes, i.e. small travel distance. Assuming z is large, then eqn (10) would produce a negative frequency, which is not valid.

CONCLUSIONS

A difference between the speed of sound of a medium and the assumed speed of sound in the beam former of an ultrasound scanner not only causes misregistration of the position of a point target in the ultrasound image, but also causes the dynamic receive focus to miss the target. The result is a broadening of the lateral pulse-echo profile of a target image. Urethane phantoms are examples of a media having a speed of sound lower than that assumed in most scanners. With the 200% to 500% increase in beam width

due to the 6% error in speed of sound, the effect of an attenuation difference on the lateral profile can be neglected for the urethane phantom.

Acknowledgements—We are grateful to Dr. Yadong Li for assistance with computer modeling. This research was supported in part by NIH grant R01CA39224.

REFERENCES

Bamber JC. Attenuation and absorption. In: CR Hill, ed. Physical Principles of Medical Ultrasonics. New York: Halsted Press, 1986: 118–199.

Dudley NJ, Gibson NM, Fleckney MJ, Clark PD: The effect of speed of sound in ultrasound test objects on lateral resolution. Ultrasound Med Biol 2002;28:1561–1564.

Goldstein A: The effect of acoustic velocity on phantom measurements. Ultrasound Med Biol 2000;26:1133–1143.

Li Y, Zagzebski JA: A Frequency Domain Model for Generating B-Mode Images with Array Transducers. IEEE Trans Ultrason Ferroel Freq Cont 1999;46:690–699.

Zagzebski JA. Essentials of Ultrasound Physics. St. Louis: Mosby-Year Book, 1996.

Zagzebski JA, Madsen EL. Ultrasound Phantoms-Concepts and Construction. In: Goldman; LW Fowlkes, ed. JB Medical CT and Ultrasound: Current Technology and Applications. Madison: Advanced Medical Publishing, 1995: 121–142.